

# Gapless insulating edges of dirty interacting topological insulators

Yang-Zhi Chou,\* Rahul M. Nandkishore, and Leo Radzihovsky  
*Department of Physics and Center for Theory of Quantum Matter,  
 University of Colorado Boulder, Boulder, Colorado 80309, USA*  
 (Dated: November 25, 2018)

We demonstrate that a combination of disorder and interactions in a two-dimensional bulk topological insulator can generically drive its helical edge *insulating*. We establish this within the framework of helical Luttinger liquid theory and exact Emery-Luther mapping. The gapless glassy edge state spontaneously breaks time-reversal symmetry in a ‘spin glass’ fashion, and may be viewed as a *localized* state of solitons which carry half integer charge. Such a qualitatively distinct edge state provides a simple explanation for heretofore puzzling experimental observations. This phase exhibits a striking non-monotonicity, with the edge growing less localized in both the weak and strong disorder limits.

## I. INTRODUCTION

Symmetry protected topological (SPT) phases, of which topological insulators [1] are the archetypal examples, are ground states of quantum matter that are ‘gapped’ insulators in the bulk, but have symmetry-enforced exotic surface properties [2, 3]. The conventional wisdom holds that at the boundary of a topological insulator there exist metallic surface states, protected by time reversal (TR) symmetry. For two-dimensional topological insulators [1, 2, 4, 5], the metallic edge is expected to support perfect ballistic conduction, and has been proposed to realize Majorana and  $Z_4$  parafermion zero modes when placed in proximity to a superconductor [6–9], opening the door to entirely new quantum technologies. A more sophisticated understanding of SPT phases also allows for the possibility of *gapped* edges, as long as the gapped edge either exhibits topological order or breaks the protecting symmetry [3]. Are the above possibilities of a gapless ballistic or gapped edge exhaustive?

In fact, experiments suggest a richer set of possibilities [11–22]. Specifically, while short and intermediate length samples of two-dimensional topological insulator indeed exhibit quantized ballistic transport, longer samples show conductance well below  $e^2/h$  per edge [11, 14, 21]. Furthermore, insulating transport was reported in InAs/GaSb [15, 17], whereas InAs/GaSb [14] and HgTe/CdTe [22] show metallic transport that appears to be robust to time-reversal (TR) symmetry breaking external magnetic field. This rich experimental phenomenology motivates a re-examination of the dogma that two dimensional topological insulators must have either a gapped or a perfect metallic edge.

In this article, we show, using nonperturbative analyses on a minimal model, that two dimensional topological insulators can exhibit a third possibility: a *gapless, insulating* edge. This possibility - which runs counter to prevailing wisdom on SPT phases in general and topological

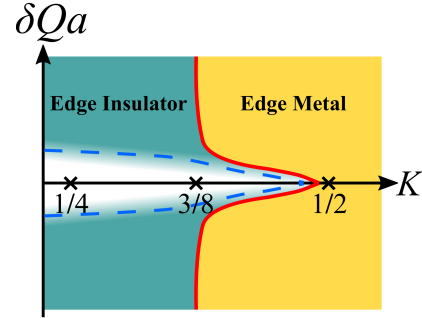


FIG. 1. The phase diagram of a disordered, interacting edge state of a 2D topological insulator. The horizontal axis is the Luttinger parameter,  $K$ , which encodes the interaction.  $K = 1$  is the non-interacting limit and  $K = 1/4$  is the strongly repulsive, exactly solvable Luther-Emery point. The vertical axis is the measure of the incommensuration  $\delta Q = (4k_F - Q)$  between electron and ion densities, with  $Q$  the reciprocal lattice vector. The red solid curve denotes the phase boundary between the gapless insulating edge (green region) and the helical ballistic edge. The gapless edge insulator corresponds to the quantum glass edge state identified in this paper, which is a Bose-glass phase [10] of helical edge bosons. A commensurate gapped insulating edge state (white shaded region), that is stable for weak bounded disorder, is rendered gapless by Lifshitz tails for strong or unbounded disorder. In the latter case, there are only two phases, a glassy insulating edge and the helical Luttinger liquid edge, with a crossover inside the glassy phase (blue dashed line) which is further illustrated in Fig. 4.

insulators in particular - becomes available through an interplay between disorder and interactions. Given that theoretical analyses seldom simultaneously treat both disorder and interactions, it is unsurprising that this possibility has not been emphasized. Nevertheless, *experimental* systems are invariably both disordered and interacting, and thus for real materials, gapless insulating edges are a generic possibility.

We focus on the boundary of a two dimensional TR-invariant topological insulator, which we model by helical Luttinger liquid theory [4, 23, 24]. This provides a natural (and nonperturbative) way to incorporate the ef-

\* YangZhi.Chou@colorado.edu

fect of short-range interactions. We then study the effect on the interacting edge states of TR-invariant disorder. This problem is very different from the conventional disordered spinless Luttinger liquid, where Anderson localization dominates the low temperature physics, in that the famous ‘topological protection’ of surface states [2] forbids conventional single particle backscattering. As a result, a minimal model of the 2D topological insulator edge state only contains perturbations from the forward scattering disorder [25] and the umklapp interaction. Forward scattering disorder alone has no effect on transport (it generates nontrivial Luttinger parameter  $K$ ). Meanwhile, the umklapp interaction can spontaneously break TR symmetry and open a gap at special (commensurate) fillings, but is irrelevant in the renormalization group (RG) sense at generic (incommensurate) filling. Thus, under generic conditions, neither forward scattering nor umklapp interactions *alone* should affect transport.

However, as we will show below, forward scattering and umklapp interactions *together* give rise to a gapless, insulating edge. In essence, umklapp interaction produces the backscattering, which disorder alone is ‘topologically prohibited’ from doing, while disorder locally compensates for the momentum mismatch (incommensuration). As a result, the *combination* of disorder and interactions can accomplish what neither can alone, giving rise to an entirely new state on the edge, which is gapless and insulating. This phase *locally* breaks TR symmetry, but in a ‘spin glass’ [26] fashion, where the ‘sign’ of the TR symmetry breaking order parameter is spatially random. It preserves *statistical* TR symmetry, (i.e. after spatial or disorder averaging), but is *localized* [27] and therefore insulating. Being localized, this state is stable to non-zero energy densities, in a manifestation of localization protected order [28], with the added subtlety that the order is itself required to enable localization [29].

The possibility of glass-like TR breaking in the ground state was anticipated already in Ref. 23 and 24. However, they focused on non-generic commensurate filling, at which interactions gap out the edge (as explicitly predicted in Ref. 23), thereby precluding the *gapless* insulating edge predicted here. While the possibility of a gapless insulating edge follows naturally from the observations in Ref. 23 and 24, as far as we are aware it has not been explored in the literature.

Here we explore the possibility of a gapless insulating edge and its phenomenology via Luttinger liquid and exact Luther-Emery analyses. We arrive at the following key results: (a) the edge is a “non-Fermi” glass [30] best thought of as a localized state of edge solitons with half-integer charge, (b) the localization length exhibits a striking non-monotonic dependence on the strength of disorder, predicting weakening of localization at both weak and strong disorder, and (c) a distinctive phenomenology, providing a natural interpretation of a number of current experiments on edge transport in topological insulators [14, 15, 21, 31].

## II. MODEL

At the edge of a two-dimensional topological insulator, there arise counter-propagating states of right ( $R$ ) and left ( $L$ ) moving fermions, that are helicity eigenstates. At low energies, the ‘kinetic energy’ part of the Hamiltonian takes the form

$$\hat{H}_0 = -iv_F \int dx [R^\dagger(x) \partial_x R(x) - L^\dagger(x) \partial_x L(x)], \quad (1)$$

where  $v_F$  is the Fermi velocity. This Hamiltonian possesses an anti-unitary time-reversal symmetry under which  $R(x) \rightarrow L(x)$ ,  $L(x) \rightarrow -R(x)$ , and  $i \rightarrow -i$ , encoding the underlying spin-1/2 structure. This symmetry rules out conventional backscattering (e.g.,  $R^\dagger L + L^\dagger R$  in the spinless Luttinger liquid) <sup>1</sup>. Disorder thus gives rise to purely ‘forward scattering’, which adds to the Hamiltonian a term

$$\hat{H}_V = \int dx V(x) [R^\dagger(x) R(x) + L^\dagger(x) L(x)]. \quad (2)$$

For analytical convenience, we take the potential  $V(x)$  to be a zero mean Gaussian random field, fully characterized by  $\overline{V(x)V(y)} = \Delta \delta(x-y)$ , where  $\overline{\phantom{x}}$  denotes a disorder average of  $\mathcal{O}$ . Additionally, short-range interactions give rise to two-particle umklapp backscattering (consistent with TR symmetry),

$$H_U = U \int dx [e^{-i\delta Q x} L^\dagger(x+\alpha) L^\dagger(x) R(x) R(x+\alpha) + \text{H.c.}], \quad (3)$$

where a point splitting with the ultraviolet length  $\alpha$  is performed. Here  $U > 0$  is the strength of the two-particle backscattering interaction and

$$\delta Q = Q - 4k_F \quad (4)$$

measures the mismatch (lack of commensuration) between electron and ion density,  $Q = 2\pi/a$  with  $a$  the lattice constant.

Employing standard bosonization [35–37] to treat the interaction nonperturbatively, the system is characterized by an imaginary-time action  $\mathcal{S} = \mathcal{S}_0 + \mathcal{S}_V + \mathcal{S}_U$  for a phonon-like field  $\theta$ , where

$$\mathcal{S}_0 = \int d\tau dx \frac{1}{2\pi v_F K} [(\partial_\tau \theta)^2 + v^2 (\partial_x \theta)^2], \quad (5a)$$

$$\mathcal{S}_V = \int d\tau dx V(x) \frac{1}{\pi} \partial_x \theta, \quad (5b)$$

$$\mathcal{S}_U = \tilde{U} \int d\tau dx \cos[4\theta - \delta Q x], \quad (5c)$$

<sup>1</sup> Technically, impurity backscattering terms with extra derivatives are allowed by TR operation. Such terms do arise in the presence of Rashba spin orbit coupling [32–34], but they do not modify the ballistic transport by themselves [1, 25].

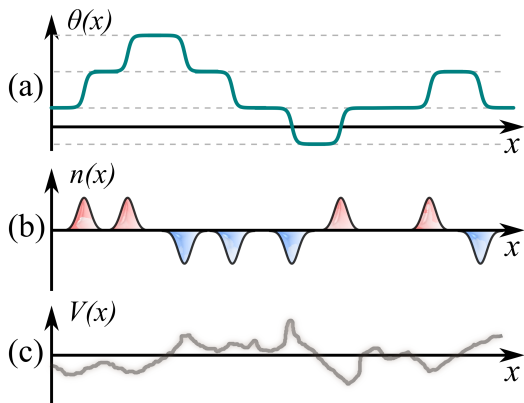


FIG. 2. Domain wall proliferation in the presence of disorder. (a) The configuration of  $\theta(x)$ . (b) The associated density profile. (c) The disorder potential. The value of  $\theta$  is restricted to  $\theta = (2N + 1)\pi/4$  (integer  $N$ ) for minimizing the  $\mathcal{S}_U$  [given by Eq. (5c)] in the clean case. In the presence of disorder, frozen-in domain walls appear, corresponding to solitons (red shaded density bump) and anti-soliton (blue shaded density depletion), and lead to spatial wandering of  $\theta$  between equivalent minima. These excitations carry half of an electron charge [38]. The solitons and the anti-solitons are “pinned” by disorder potential  $V(x)$  [sketched in (c)], leading to the quantum ‘spin-glass’ edge state, which may be viewed as a localized state of these domain-walls.

with  $v$  the velocity of the boson,  $K$  the Luttinger parameter,  $\tilde{U} = U/(2\pi^2\alpha^2)$ , and  $\alpha$  an ultraviolet length scale<sup>2</sup>. For a system with repulsive interactions  $K < 1$  ( $K = 1$  being the non-interacting point). The bosonized form of the long-lengthscale part of electron density is given by  $n = \partial_x \theta / \pi$ . We take the disorder and interactions to be sufficiently weak, that they do not close the *bulk* gap, i.e., the bulk topological insulator phase is stable.

### III. QUANTUM GLASS STATE

In the clean system [ $V(x) = 0$ ] with commensuration ( $\delta Q = 0$ ), the two-particle backscattering in Eq. (5c) is relevant for  $K < 1/2$  [36]. It spontaneously breaks the TR symmetry at zero temperature [23], and opens up a gap at the edge. However, (a) commensuration is unlikely in typical samples, requiring fine-tuning, (b) spontaneous ordering of this sort will not survive to non-zero temperatures [39], and (c) general arguments [40] establish that such a long-range ordered state is unstable to arbitrarily weak disorder in one dimension.

In the absence of disorder, but at incommensurate electron density ( $\delta Q \neq 0$ ), weak two-particle backscat-

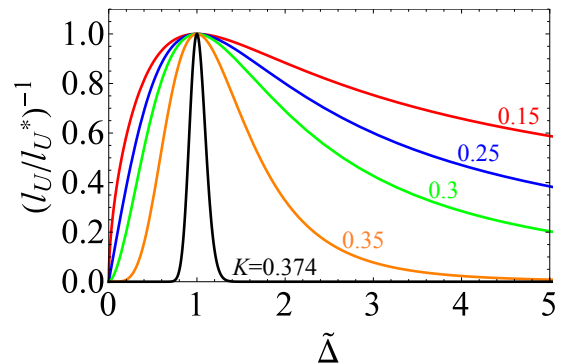


FIG. 3. The inverse localization length as a function of disorder. The localization length  $l_U$  shows non-monotonic behavior as a function of the dimensionless parameter,  $\tilde{\Delta} = 8K^2\Delta/(v^2\delta Q)$ , which measures disorder strength. Here  $l_U$  is extracted via RG analysis,  $l_U \sim \alpha\Delta_U^{-1/(3-8K)}$ , and  $l_U^*$  is the smallest value of the localization length with fixed values of  $\delta Q$  and  $\tilde{U}$ . Different values of the Luttinger parameters are plotted in black ( $K = 0.374$ ), orange ( $K = 0.35$ ), green ( $K = 0.3$ ), blue ( $K = 0.25$ ), and red ( $K = 0.15$ ) curves. Regardless of the interaction, the localization length diverges both in the zero disorder limit and in the infinite disorder limit.

tering,  $\mathcal{S}_U$  is formally irrelevant due to kinematic constraints from momentum conservation. The symmetry and the gapless edge will be restored by sufficiently large incommensuration  $|\delta Q| > \delta Q_c$ , via a commensurate-incommensurate phase transition [41]. In the presence of disorder, however, the kinematic constraint is relaxed, and the backscattering can be enhanced. To treat the combination of interaction and disorder rigorously, we first perform a change of variable,  $\theta(x) \rightarrow \theta(x) - \frac{K}{v} \int_{-\infty}^x ds V(s)$ , to eliminate the  $\mathcal{S}_V$  term. Then  $\mathcal{S}_U$  becomes

$$\mathcal{S}_U = \frac{\tilde{U}}{2} \int d\tau dx \left\{ \eta(x) e^{i4\theta(\tau,x)} + \eta^*(x) e^{-i4\theta(\tau,x)} \right\} \quad (6a)$$

$$= \tilde{U} \int d\tau dx \cos[4\theta(x) + \chi(x)], \quad (6b)$$

where  $\eta(x) = e^{i\chi(x)}$ ,  $\chi(x) = -\frac{4K}{v} \int_{-\infty}^x ds V(s) - \delta Qx$ , with random-field Gaussian statistics characterized by  $\overline{\eta^*(x')\eta(x)} = e^{-\frac{8K^2}{v^2}\Delta|x-x'|} e^{-i\delta Q(x-x')}$ ,  $\overline{\eta(x')\eta(x)} = 0$ ,  $\overline{\eta(x)} = 0$ . Here  $\mathcal{S}_U$  given by Eq. (6) is an umklapp two particle backscattering with a position-dependent random phase  $\chi(x)$  executing a random walk<sup>3</sup>. This effective random-field XY model maps to the Bose-glass problem analyzed in [10, 42], and supports a glassy (i.e. insulating) phase. In the presence of Gaussian disorder,

<sup>2</sup> A generic model would also include a (TR symmetry allowed) random two particle backscattering, leading to a short range correlated random contribution to the coefficient  $\tilde{U}$  in Eq. (5c). As long as  $\tilde{U}(x)$  has non-zero mean (arising from interactions) the behavior remains qualitatively the same.

<sup>3</sup> The random two particle backscattering terms were first obtained from symmetry analysis in Ref. 23 and 24. Note however that the backscattering term in Eq. (6b) contains a uniform amplitude, which is different from those in Ref. 23 and 24.

the gap will be smeared out, although a strong crossover controlled by Lifshitz tails will survive at weak disorder, illustrated in Figs. 1 and 4.

To treat the disordered-assisted umklapp action  $\mathcal{S}_U$  [given by Eq. (6)] we employ a replica method [26] (equivalent to the Keldysh formalism), which allows us to average over disorder, generating a replicated (effectively) translationally-invariant action (see Ref. 43 and Appendix C),

$$\mathcal{S}_{U,dis} = -\Delta_U \sum_{a,b} \int d\tau d\tau' dx \cos[4(\theta_a(\tau, x) - \theta_b(\tau', x))]. \quad (7)$$

Here,

$$\Delta_U = \tilde{U}^2 \frac{K^2 \Delta / v^2}{16(K^2 \Delta / v^2)^2 + \delta Q^2 / 4}, \quad (8)$$

and  $a, b$  are replica indices, with the standard zero-replica limit to be taken at the end of the computation. Note that the argument of the cosine in Eq. (7) is insensitive to incommensuration. Intuitively, disorder takes care of the commensuration by ‘supplying the missing momentum’ to make the interaction locally commensurate. We note in passing that this ‘positive feedback’ has been previously discussed in the context of finite temperature transport in the perturbative regime [43–45].

Although the physical origin of the disorder-assisted interaction is quite different,  $\mathcal{S}_{U,dis}$ , is formally identical to the random single-particle backscattering in the Giamarchi-Schulz model, with rescaling  $\theta \rightarrow 2\theta$ , corresponding to  $K \rightarrow 4K$  [43]. It follows from a standard analysis that this operator becomes relevant for  $K < 3/8$  [23, 24, 42], driving an instability to a Bose-glass phase, corresponding to a gapless localized edge, as we discuss below. An estimate for the localization length in the glass phase may be obtained from the RG analysis [36, 42] that predicts a length scale  $l_U \sim \alpha \Delta_U^{-1/(3-8K)} \propto U^{-2/(3-8K)}$  at which the disorder assisted umklapp becomes strong. We further note that the localized nature of the edge can stabilize order to non-zero energy densities [28].

To discuss the nature of the glassy edge state we note that forward-scattering disorder forces  $\theta(x)$  to jump between degenerate minima of Eq. (5c) whenever  $V(x)$  locally exceeds the critical  $\delta Q_c$  (corresponding to the soliton gap), thereby producing a random distribution of domain walls, as illustrated in Fig. 2 (for a detailed discussion see Appendix D). Note that domain walls connect two states related by TR operation, and are characterized by a  $\pi/2$  change in  $\theta$ . Since the charge density is  $\frac{e}{\pi} \partial_x \theta$  it follows that the domain walls are fractionalized charge  $e/2$  excitations [38]. The glassy edge state is best thought of as a ‘localized state of domain walls’ rather than of bare fermions, and as such may be viewed as an example of a ‘non-Fermi glass’ [30]. Note that such a localized state of domain walls spontaneously breaks TR symmetry in a spatially random fashion.

We emphasize that effective strength of the disorder assisted umklapp backscattering  $\Delta_U(\Delta)$  in Eq. (8) is a non-monotonic function of  $\Delta$ . (Also see Fig. 3 for inverse localization length.) Clearly the effects of disorder increase with  $\Delta$  at small disorder, with the edge being ballistic in the zero disorder limit. Meanwhile, it follows from inspection of Eq. (5b) that  $V(x)$  (viewed as a smoothly varying function) locally increases incommensuration (adding a random contribution to  $\delta Q$  in Eq. (5c), thereby locally proliferating domain walls). For typical  $V(x) > v\delta Q$  this has the effect of suppressing umklapp backscattering. Since  $\Delta$  represents the typical strength of  $V(x)$ , it follows that localization should paradoxically get *weaker* as  $\Delta$  is increased in the strong disorder regime.

A more rigorous treatment of the strong-coupling phase may be obtained by re-fermionizing the model given by Eq. (5) at the Luther-Emery point ( $K = 1/4$ ). The corresponding Luther-Emery Hamiltonian is given by

$$\begin{aligned} \hat{H}_{LE} = & -iv \int dx [\Psi_R^\dagger \partial_x \Psi_R - \Psi_L^\dagger \partial_x \Psi_L] \\ & + M \int dx [\Psi_R^\dagger \Psi_L + \Psi_L^\dagger \Psi_R] \\ & - \frac{1}{2} \int dx [V(x) + v\delta Q] [\Psi_R^\dagger \Psi_R + \Psi_L^\dagger \Psi_L], \quad (9) \end{aligned}$$

where  $M = U/(2\pi\alpha)$  is the mass of Luther-Emery fermion. Note that in this representation, the problem has simplified to a non-interacting theory with disorder.

The Luther-Emery fermion obeys a massive Dirac equation with a spatially inhomogeneous scalar potential  $V(x)/2$ . The corresponding variance of the scalar potential  $V(x)/2$  is  $\tilde{\Delta} = \Delta/4$ . The problem of a non-interacting massive fermion with scalar potential disorder is exactly solvable [46], and exhibits localization for arbitrarily weak disorder at all energies (i.e. for arbitrary incommensuration  $\delta Q$ ). For unbounded disorder, there is no gap in the density of states. Nevertheless in the weak disorder limit  $\tilde{\Delta}/(Mv) \ll 1$ , the subgap density of states is exponentially small, whereas for strong disorder  $\tilde{\Delta}/(Mv) \gg 1$ , the gap is completely smeared out, leading to a crossover driven by disorder strength which is illustrated in Fig. 4. For weak bounded disorder, a distinct gapped phase survives.

The physical density and current operators can be written in terms of the Luther-Emery fermion fields:  $n = \frac{e}{2} (\Psi_R^\dagger \Psi_R + \Psi_L^\dagger \Psi_L)$  and  $j = \frac{ev}{2} (\Psi_R^\dagger \Psi_R - \Psi_L^\dagger \Psi_L)$ , where  $e < 0$  is the charge of an electron. Since these fermions (which carry half integer charge) are localized, it follows that the physical conductivity vanishes. Meanwhile, the absence of a hard gap for the Luther-Emery fermions implies that the physical compressibility is always nonzero. Thus the edge is a localized compressible state of Luther-Emery fermions, which in turn correspond to domain walls of  $\mathcal{S}_0 + \mathcal{S}_U$  [given by Eq. (5)] in the language of bosonization. We thus conclude, that at  $K = 1/4$ , consistent with the bosonization arguments



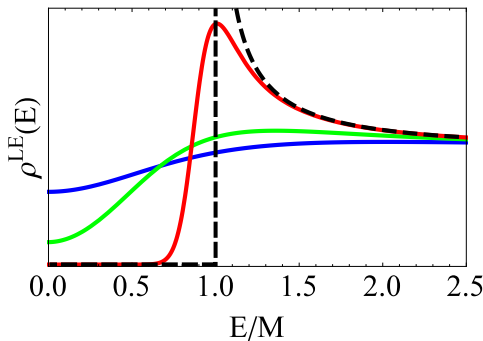


FIG. 4. The disorder-averaged density of states of Luther-Emery fermions with Hamiltonian Eq. (9) based on the analytic solution in Ref. 46, for a range of variances,  $\tilde{\Delta}/(Mv) = 0.1, 0.5, 1$  (red, green, blue respectively) of Gaussian disorder potential. The black dashed line is the disorder-free density of states. For unbounded disorder (e.g., Gaussian) distributions, the density of states is nonzero for arbitrarily small  $\Delta$ , due to exponentially small subgap Lifshitz tails, a relic of a Mott insulator in the clean edge.

there arises a localized state of domain walls, for arbitrary filling  $\delta Q$  and even at weak disorder, which generically manifests as a gapless insulating edge.

Note that  $V(x)$  in Eq. (9) plays a dual role: it both introduces disorder and acts as a local chemical potential, increasing the density of effective fermions. Away from the Luther-Emery point  $K = 1/4$ , the effective fermions are interacting, and the Anderson insulator grows less stable to interactions with increasing density. It then follows that increasing disorder beyond an optimal value set by  $\delta Q$  strikingly weakens localization on the edge. This provides a complementary perspective on the aforementioned non-monotonicity [Eq. (8) and Fig. 3] of the effects of disorder.

#### IV. EXPERIMENTAL SIGNATURES OF QUANTUM GLASS EDGE

Having established the insulating glass nature of the disordered interacting edge of the topological insulator, many experimental predictions then follow from general understanding of randomly-pinned and driven elastic media, (e.g., charge-density waves [47–51]), and quantum transport in the localized state [52].

Owing to the glassy insulating nature of the edge, at zero temperature, a finite length  $L$  sample will be characterized by a dc conductance  $G \sim (e^2/h)e^{-L/l_v}$  per edge, vanishing in thermodynamic limit. We expect the corresponding ac conductivity to be described by a Mott form  $\sigma(\omega) \sim \omega^2$  for low frequency, and non-universal power law dependence  $\sigma(\omega) \sim \omega^{-4+8K}$  for the high frequency tail [49].

Quite generically we therefore expect that at zero temperature, above a threshold electric field, the glassy edge will exhibit a collective depinning transition from

an insulating to a conducting state, studied extensively in the context of charge-density waves [47–51]. We thus predict a nonlinear I-V characteristic for the low-temperature edge transport. Concomitantly, we expect above-threshold transport to exhibit narrow-band noise and mode-locking phenomena at characteristic frequency  $\omega \sim eV/\hbar$ , set by voltage,  $V$ .

In addition to transport measurements, there are a couple of experimental protocols that reveal the properties of quantum glass states. Compressibility measurement can confirm the gaplessness. Scanning tunneling microscopy, which measures the local density of states, can tell a gapless state and provide spatial distribution of electrons in a fixed energy. The half charge nature can in principle be probed through Coulomb blockade [38]. Charge density autocorrelation functions on the edge should find glassy dynamics. Non-local charge response [53] on the edge also gives distinct signatures of the localized state.

#### V. DISCUSSION AND CONCLUSION

We have shown that an interacting edge of a topological insulator with symmetry-preserving disorder can exhibit a quantum glass phase that spontaneously breaks time-reversal symmetry. This phase is a gapless compressible insulator that corresponds to a Bose-glass of the phonon-like field  $\theta$  [10], or equivalently a localized state of domain walls of  $\theta$ . This constitutes a qualitatively new possibility for the edge of a two-dimensional topological insulator (and more generally, SPT phases), distinct from a metallic or a gapped edge. Insofar as this state is localized, it can survive to non-zero energy density. The corresponding phase diagram is sketched in Fig. 1.

This new phase provides an alternative perspective on existing experiments [12, 14, 15, 21, 31], as we will now discuss. In order to make a meaningful comparison to experiments, we must first discuss the evolution of the glassy edge state in applied magnetic field. How is the transport behavior altered if we explicitly break TR symmetry by applying external magnetic field? Inside the glassy phase the edge is already localized and TR symmetry is spontaneously broken. Thus, applying weak external field has little effect - it simply shifts the localization length, as shown in Fig. 5 (b). In contrast, application of magnetic field to the TR invariant metallic state triggers a phase transition to an insulator [see Fig. 5 (a)], which in non-interacting limit is simply an Anderson insulator of electrons [54]. A detailed analysis of the effects of applied field within the language of bosonization is provided in Appendix E. We summarize here the key results.

Application of magnetic field  $B$  to the metallic TR preserving state leads to the conductance

$$G = \frac{e^2}{h} e^{-L/l_B}, \quad (10)$$

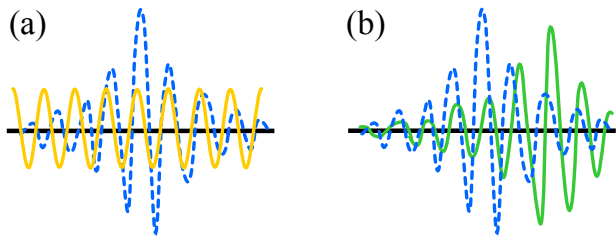


FIG. 5. Schematic illustration of the modification of the wavefunction in the presence of external magnetic field. (a) The sketched wavefunctions for  $K > 3/8$ . The yellow curve represents a delocalized wavefunction which corresponds to ballistic transport. In the presence of magnetic field, the wavefunction becomes localized (blue dash curve). (b) The sketched wavefunction for  $K < 3/8$ . In the absence of magnetic field, the ground state is a quantum glass (green curve) which is a gapless TR breaking insulator. The state remains localized upon turning on magnetic field (blue dash curve).

where  $l_B \propto B^{-2/(3-2K)}$ , recovering ballistic transport when  $L \ll l_B$ , where  $L$  is the length of the sample. Application of magnetic field to the glassy TR breaking state proposed here (stable for  $K < 3/8$  at generic incommensurate electron density) leads to the conductance

$$G = \frac{e^2}{h} e^{-L/l_{\text{loc}}}, \quad (11)$$

with  $l_{\text{loc}} = \min(l_B, l_U)$ . This crosses over to Eq. (10) only for  $B > B_*$  (when  $l_B < l_U$ ), where

$$B_* \sim l_U^{K-3/2} \sim \Delta_U^{\frac{3/2-K}{3-8K}} \quad (12)$$

is the crossover magnetic field below which the system is insensitive to magnetic field  $B$ .

How do these predictions compare with experiment? In InAs/GaSb insulating behavior is observed in the absence of external magnetic field [15, 17]. The samples are strongly interacting with estimated Luttinger parameter  $K \sim 0.2$  [15] owing to the small Fermi velocities [12, 14]. In this  $K < 3/8$  regime our theory indeed predicts a gapless insulating edge, consistent with these experimental observations.

In InAs/GaInSb samples [21, 31], conducting behavior is observed, but with conductance less than  $e^2/h$  for long samples in the absence of applied magnetic field. In the presence of applied magnetic field, resistivity increases sharply. In these samples the estimated Luttinger parameters are roughly 0.4-0.5 [21, 31], close to but greater than our critical value  $K = 3/8 = 0.375$ . Thus, we do expect conducting behavior in these samples, with a transition to insulating behavior driven by applied magnetic field. We conjecture that the less than ballistic transport observed in these samples (in the absence of applied field) may be due to rare regions with  $K < 3/8$ <sup>4</sup>, which

locally break the time-reversal symmetry spontaneously and provide finite resistivity. Of course, the TR symmetry is still approximately restored for any finite temperature [23] when the system is coupled to an external heat bath (e.g. phonons).

We note that conducting edges were reported in HgTe/CdTe [22] even in the presence of magnetic field. This material is believed to be weakly interacting ( $K \sim 0.8$  [55]). This observation does not have a natural explanation within our theory, but might be understood by material specific issues [56, 57].

We comment briefly on some of the other explanations that have been proffered for the experiments. One explanation that has been advanced for resistive behavior [17] is that the system may simply be in the trivial phase, without a topologically protected edge. Even if the sample is in the topological phase, strong interaction can open up a gap and spontaneously break TR symmetry [23], leading to an insulating behavior. However, this requires fine-tuning to commensuration and assumes a disorder-free system. There are also theories that are specific to particular material realizations [56–59]. Unlike all these, our analysis indicates that the TR-breaking edge state is a robust and generic feature of the strongly interacting 2D topological insulator edge states.

Another possibility that has been discussed in the literature is charge puddles near the edge [60, 61]. These can behave like a Kondo impurities [61–63] and can generate insulator-like finite-temperature conductivity [64]. An extensive number of the Kondo impurities can also localize the helical edge state by spontaneously breaking the time-reversal symmetry [65]. Our mechanism bears some family resemblance to these, but differs crucially in that there is no need to invoke additional gapless states (such as charge puddles) in the *bulk*, nor to invoke effectively magnetic impurities - our scenario applies even to the pure one dimensional edge of a topological insulator that is fully gapped in the bulk, with purely TR-preserving disorder on the edge. We conclude that our theory of a gapless insulating edge provides a *simple* explanation for a number experimental observations, independent of material and bulk details, and sensitive only to the edge theory. As a non-trivial *prediction* of our theory, the glassy edge state that we identify should exhibit a non-monotonic dependence on disorder strength, being maximally insulating (i.e. having shortest localization length) at *intermediate* disorder strengths (Fig. 3). Moreover the localized objects are solitons with half integer charge.

Thus, we have shown that topological insulators *can* have gapless insulating edge states. This scenario also provides a simple explanation of apparent experimental anomalies. While our present analysis was restricted to topological insulators in two dimensions, a generalization to higher dimensional systems and more general SPT phases should follow *mutatis mutandis*. We leave this, as well as a re-examination of other experiments through this lens, as a challenge for future work.

<sup>4</sup> Spatially inhomogeneous Luttinger parameter can arise in the presence of random Rashba spin orbit coupling [25].

## ACKNOWLEDGEMENTS

We thank Ravin Bhatt, Charles Kane, Jed Pixley, Michael Pretko, Abhinav Prem, and Hong-Yi Xie for useful discussions and feedback. This work is supported in part by a Simons Investigator award from the Simons Foundation, and NSF grant no. DMR-1001240 (Y.-Z.C. and L.R.), and in part by the Army Research Office under Grant Number W911NF-17-1-0482 (Y.-Z. C. and R.N.). The views and conclusions contained in this document are those of the authors and should not be interpreted as representing the official policies, either expressed or implied, of the Army Research Office or the U.S. Government. The U.S. Government is authorized to reproduce and distribute reprints for Government purposes notwithstanding any copyright notation herein.

## Appendix A: Bosonization Convention

We adopt the standard field theoretic bosonization method [35, 37]. The fermionic fields can be described by chiral bosons via

$$R(x) = \frac{1}{\sqrt{2\pi\alpha}} e^{i[\phi(x)+\theta(x)]}, \quad L(x) = \frac{1}{\sqrt{2\pi\alpha}} e^{i[\phi(x)-\theta(x)]}, \quad (\text{A1})$$

where  $\alpha$  is the ultraviolet length scale that is determined by the microscopic model. The time-reversal operation ( $\mathcal{T}^2 = -1$ ) in the bosonic language is defined as follows:  $\phi \rightarrow -\phi + \frac{\pi}{2}$ ,  $\theta \rightarrow \theta - \frac{\pi}{2}$ , and  $i \rightarrow -i$ . This corresponds to the fermionic operation:  $R \rightarrow L$ ,  $L \rightarrow R$ , and  $i \rightarrow -i$ .

On the contrary, the non-topological spinless fermion obeys the time-reversal operation ( $\mathcal{T}^2 = +1$ ). The fermionic operation is  $R \rightarrow L$ ,  $L \rightarrow R$ , and  $i \rightarrow -i$ . The operation does not forbid the conventional backscattering term,  $R^\dagger L + L^\dagger R$ , which admits Anderson localization.

## Appendix B: Rashba spin-orbit coupling and TR breaking order parameters

The TR operation  $\mathcal{T}^2 = -1$  forces ‘masses’ in the helical Luttinger liquid to break TR symmetry. This is because the helical Luttinger liquid still contains the parent ‘spinful’ feature in the bulk (even though spin is not necessarily a good quantum number). We briefly discuss the connection between physical fermion and the edge chiral fermions (right and left movers).

In a generic 2D topological insulator, the physical electron field can be expanded as [25, 34]

$$\begin{aligned} c_\uparrow(x) &\approx e^{ik_F x} R(x) - i\zeta e^{-ik_F x} \partial_x L(x), \\ c_\downarrow(x) &\approx e^{-ik_F x} L(x) - i\zeta^* e^{ik_F x} \partial_x R(x), \end{aligned} \quad (\text{B1})$$

where  $\zeta$  is a phenomenological parameter that encodes the Rashba spin orbit coupling. The TR operation:

$c_\uparrow \rightarrow c_\downarrow$ ,  $c_\downarrow \rightarrow -c_\uparrow$ , and  $i \rightarrow -i$ . The quantum spin Hall insulator corresponds to  $\zeta = 0$  due to the absence of Rashba spin orbit coupling. The electron density operator is expressed as

$$\begin{aligned} n &= c_\uparrow^\dagger c_\uparrow + c_\downarrow^\dagger c_\downarrow \\ &\approx R^\dagger R + L^\dagger L - \{i\zeta e^{-i2k_F x} [R^\dagger \partial_x L - (\partial_x R^\dagger) L] + \text{H.c.}\}, \end{aligned} \quad (\text{B2})$$

where we only keep the leading  $O(|\zeta|)$  terms. The  $2k_F$  component of the density operator contains unconventional backscattering. As pointed out in Ref. 25, the effect of these backscattering term can be dealt with change of basis, and the helical edge state remains backscattering-free in the new ‘rotated frame’.

The spin-flip bilinears are expressed as follows:

$$c_\uparrow^\dagger c_\downarrow \approx e^{-i2k_F x} R^\dagger L + i\zeta^* (\partial_x L^\dagger) L - i\zeta^* R^\dagger \partial_x R, \quad (\text{B3})$$

$$c_\downarrow^\dagger c_\uparrow \approx e^{i2k_F x} L^\dagger R + i\zeta (\partial_x R^\dagger) R - i\zeta L^\dagger \partial_x L, \quad (\text{B4})$$

where we have omitted the  $O(|\zeta|)$  terms. The backscattering term  $R^\dagger L$  and  $L^\dagger R$  do carry TR breaking features as the spin-flip bilinears. However, they are not physical spin-flip operator as long as  $\zeta$  is non-zero (due to the lack of spin conservation). In bosonization, the TR breaking mass operators are expressed as follows [23]:

$$m_x = e^{i2k_F x} L^\dagger R + \text{H.c.} = \frac{1}{\pi\alpha} \sin[2\theta + (2k_F - Q)x], \quad (\text{B5})$$

$$m_y = ie^{i2k_F x} L^\dagger R + \text{H.c.} = \frac{1}{\pi\alpha} \cos[2\theta + (2k_F - Q)x], \quad (\text{B6})$$

where  $Q$  is the commensurate wavevector set by the microscopic lattice model. Finite expectation of  $m_x$  ( $m_y$ ) can be viewed as a *pseudospin* order along  $x$  ( $y$ ) direction that breaks TR symmetry.

## Appendix C: Renormalization Group Analysis

In the presence of the Gaussian unbounded forward disorder, the interaction term  $\mathcal{S}_U$  becomes irrelevant. This can be simply seen in Eq. (6). The fluctuating factor  $\eta(x)$  vanishes after the disorder average.

At second order of  $U$ ,  $\mathcal{S}_{U,dis}$  given by Eq. (7) is generated under RG flow. The precise functional form of the coupling constant  $\Delta_U$  is not very important for this study. We follow the strategy in Ref. 43. We first perform cumulant expansion of the partition function,  $\overline{e^{-\mathcal{S}}} \approx \exp\left[-\overline{\mathcal{S}} + \frac{1}{2}(\overline{\mathcal{S}^2} - \overline{\mathcal{S}}^2)\right] \equiv e^{-\mathcal{S}_U^{(1)} - \mathcal{S}_U^{(2)}}$ . The linear in  $U$  term,  $\mathcal{S}_U^{(1)}$ , vanishes exactly. The second order contribution in the action is as follows:

$$\begin{aligned} \mathcal{S}_U^{(2)} &= -\frac{1}{2} \left(\frac{\tilde{U}}{2}\right)^2 \sum_{a,b} \int d\tau dx \int d\tau' dx' e^{-\frac{8K^2\Delta}{v^2}|x-x'|} \\ &\quad \times \left\{ e^{i\delta Q(x-x')} e^{i4[\theta_a(\tau,x) - \theta_b(\tau',x')]} + \text{H.c.} \right\}, \end{aligned} \quad (\text{C1})$$

where  $a$  and  $b$  are replica indexes. The exponential decay in the first line of Eq. (C1) implies that the long wavelength physics can be treated as effective white noise correlated problem, similar to the backscattering term in the Giamarchi-Schulz model [23, 24, 42]. In order to see this explicitly, we integrate over the relative spatial degrees of freedom,  $r = x - x'$ , to compute  $\Delta_U$ .

$$\Delta_U = \frac{1}{4} \tilde{U}^2 \int_{-\infty}^{\infty} dr e^{-8 \frac{K^2 \Delta}{v^2} |r|} e^{i \delta Q r} \quad (C2)$$

$$= \tilde{U}^2 \frac{K^2 \Delta / v^2}{16 (K^2 \Delta / v^2)^2 + \delta Q^2 / 4}. \quad (C3)$$

Based on scaling analysis we obtain the RG flow equation:

$$\frac{d\Delta_U}{dl} = (3 - 8K) \Delta_U. \quad (C4)$$

Therefore, the dirty helical Luttinger liquid is stable for  $K > 3/8$  in the model given by Eq. (5). Meanwhile, for  $K < 3/8$ , backscattering is a relevant perturbation. This we interpret as an instability to localization, a conclusion that is supported by analysis of the exactly solvable Luther-Emery point  $K = 1/4$  in the main text.

#### Appendix D: Domain Wall Solution with Disorder

We first consider a sine-Gordon model in the clean limit. The action is as follows:

$$\begin{aligned} \mathcal{S}' = & \int d\tau dx \frac{1}{2\pi v K} \left[ (\partial_\tau \theta)^2 + v^2 (\partial_x \theta)^2 \right] \\ & + \tilde{U} \int d\tau dx \left\{ \cos [4\theta(\tau, x)] + 1 \right\}, \end{aligned} \quad (D1)$$

where  $\tilde{U}$  is the interaction strength. We have assumed the system is commensurate. The extra constant 1 is added in order to avoid infinity in the later calculations. The equation of motion is as follows:

$$\frac{1}{\pi v K} \left[ \partial_\tau^2 \theta + v^2 \partial_x^2 \theta \right] + 4\tilde{U} \sin [4\theta] = 0. \quad (D2)$$

Assuming no temporal fluctuation, we can construct a domain wall solution as follows:

$$\theta_X(x) = \arctan \left[ -\tanh \left( 2\sqrt{\pi \tilde{U} K / v x} \right) \right], \quad (D3)$$

where  $\theta_X(-\infty) = -\pi/4$  and  $\theta_X(\infty) = \pi/4$ . The solution  $\theta_X$  is approximately correct for a finite system with size  $L$  when  $\sqrt{\pi \tilde{U} K / v L} \gg 1$ .

We first focus on the saddle point contribution of  $\theta_X(x)$ . The partition function is approximated by  $Z \propto \sum_{x_0} e^{-\mathcal{S}[\theta_X(x-x_0)]}$  where  $x_0$  indicates the position of the domain wall. The saddle point contribution  $\mathcal{S}[\theta_X(x-x_0)]$

only weakly depends on  $x_0$ . We plug Eq. (D3) in Eq. (D1).

$$\begin{aligned} \mathcal{S}[\theta_X] = & \beta \int dx \left\{ \frac{v (\partial_x \theta_X)^2}{2\pi K} + \tilde{U} [\cos (4\theta_X) + 1] \right\} \\ = & 2\tilde{U} \beta \int dx [\cos (4\theta_X) + 1] \\ = & 2\beta \sqrt{\tilde{U} v / (\pi K)}, \end{aligned} \quad (D4)$$

where we have used Eq. (D2). The energy cost of having a domain wall is  $\Delta E = 2\sqrt{\tilde{U} v / (\pi K)}$ .

#### 1. Increased Energy Due to Disorder

Now, we consider adding a disorder action  $\mathcal{S}_V$  [given by (5b)]. We first perform a change of variable to eliminate the  $\mathcal{S}_V$ ,  $\theta(x) \rightarrow \theta(x) - \frac{K}{v} \int_{-L/2}^x ds V(s)$ . The  $\mathcal{S}'$  becomes to

$$\begin{aligned} \mathcal{S}' = & \int d\tau dx \frac{1}{2\pi v K} \left[ (\partial_\tau \theta)^2 + v^2 (\partial_x \theta)^2 \right] \\ & + \tilde{U} \int d\tau dx \left\{ \cos [4\tilde{\theta}(\tau, x)] + 1 \right\}, \end{aligned} \quad (D5)$$

where  $\tilde{\theta}(\tau, x) = \theta(\tau, x) - \frac{K}{v} \int_{-L/2}^x ds V(s)$ .

First of all, we assume that the field  $\tilde{\theta}$  is pinned by the interaction term. This means  $\theta(\tau, x) = \frac{K}{v} \int_{-L/2}^x ds V(s) + \frac{\pi}{4}(2N+1)$  with integer  $N$ . The solution minimizes the  $\tilde{U}$  term to zero. We compute the corresponding energy in the kinetic energy part

$$\delta E = \frac{v}{2\pi K} \int dx (\partial_x \theta)^2 = \frac{v}{2\pi K} \frac{K^2}{v^2} \int dx V^2(x), \quad (D6)$$

$$\rightarrow \overline{\delta E} = \frac{K}{2v\pi} \Delta L, \quad (D7)$$

where  $\overline{\delta E}$  is the averaged kinetic energy. The extra energy cost of a uniform configuration due to disorder is proportional to the system size which is even stronger than in the Imry-Ma argument [40]. Meanwhile, the energy cost of a domain wall is just a constant, as discussed above. Therefore, it is energetically favorable to locally distort to match the disorder, thereby introducing a finite density of domain walls even at zero temperature.

#### 2. Domain Wall Pinning in A Fixed Realization

We previously showed that the ground state should contain a non-zero density of domain walls. In this appendix we construct the domain wall solution in a fixed realization of disorder.

The disorder potential  $V(x)$  couples to  $\partial_x \theta$ . The domain wall solution is mostly flat except for the ‘‘thin wall’’



region. A domain wall can take place as long as the local disorder potential provide enough energy gain. This is translated into

$$\left| \int dx \frac{V(x)}{\pi} \partial_x \theta_X(x - x_0) \right| \geq 2\sqrt{\tilde{U}v/(\pi K)}, \quad (\text{D8})$$

where  $x_0$  is the position of a domain wall and  $\theta_X$  is given by Eq. (D3). The sign of the integral determines if  $\theta$  should increase or decrease in value (see Fig. 2). Based on Eq. (D8), the domain walls are pinned by the rare strong disorder regions. The ground state consists of multiple mini blocks that are separated by domain walls. Inside each block,  $\theta = (2N + 1)\pi/4$  where  $N$  is an integer. This line of reasoning predicts a ground state that breaks TR symmetry in ‘spin glass’ like fashion, with localized domain walls separating domains with different values of  $\theta$ .

### Appendix E: Effects of magnetic field

The magnetic field coupling terms at the linear order [38, 54] are as follows:

$$\begin{aligned} H_B = & t_z B_z \int dx [R^\dagger R - L^\dagger L] \\ & + t_x B_x \int dx [e^{-i2k_F x} R^\dagger L + e^{i2k_F x} L^\dagger R] \\ & + t_y B_y \int dx [-ie^{-i2k_F x} R^\dagger L + ie^{i2k_F x} L^\dagger R], \end{aligned} \quad (\text{E1})$$

where  $B_a$  is the  $a$ -component of the magnetic field,  $t_a$  is the model-dependent coupling constant for the  $a$ -component. The  $t_z$  term shifts the wavevector of the edge mode but does not induce backscattering for the weak field. For simplicity, we only consider the  $t_x$  and  $t_y$  terms that induce backscatterings of the edge states.

The corresponding bosonized action is given by,

$$\begin{aligned} \mathcal{S}_B = & \frac{t_x B_x}{\pi\alpha} \int d\tau dx \sin[2\theta(\tau, x) + (2k_F - Q)x] \\ & + \frac{t_y B_y}{\pi\alpha} \int d\tau dx \cos[2\theta(\tau, x) + (2k_F - Q)x], \end{aligned} \quad (\text{E2})$$

where  $Q$  is the commensurate wavevector set by the microscopic lattice model.

In a clean helical edge with  $K > 1/2$ , the magnetic field term  $\mathcal{S}_B$  can open up a gap when  $Q = 2k_F$ . In particular, the conductance in a non-interacting edge state ( $K = 1$ ) drops from  $G = G_0 = e^2/h$  to  $G(B) \approx G_0 e^{-m(B)L/v}$ , where  $L$  is edge length and  $m(B) \propto B$  is the gap induced by the magnetic field. On the other hand, the transport behavior does not change much in a clean edge with  $K < 1/2$  and  $Q = 2k_F$  (which implies  $4k_F$  is also commensurate). The ground state configuration is determined by minimizing  $\mathcal{S}_U + \mathcal{S}_B$  rather than  $\mathcal{S}_U$  alone. The effect of the magnetic field is to enhance the gap and change the precise ground state condition.

In the disordered case, we first examine the non-interacting limit ( $K = 1$  and  $U = 0$ ). The model corresponds to a massive Dirac fermion with a scalar potential disorder. This Dirac model gives Anderson localization for the whole spectrum [46]. The mass term is proportional to the strength of the magnetic field  $B$ . The value of  $(2k_F - Q)$  in  $\mathcal{S}_B$  determines the position of the fermi energy which does not affect the localization.

For a generic interacting edge state with disorder, we adopt the same procedure of deriving  $\mathcal{S}_{U,dis}$  in Sec. III. The new effective action is as follows:

$$\begin{aligned} \mathcal{S}_{B,dis} = & -\Delta_B \sum_{a,b} \int d\tau d\tau' dx \\ & \times \cos[2(\theta_a(\tau, x) - \theta_b(\tau', x))], \end{aligned} \quad (\text{E3})$$

where  $\Delta_B \propto B^2$ .  $\mathcal{S}_{B,dis}$  is the same as the disorder averaged backscattering term in the Giamarchi-Schulz model [42].  $\mathcal{S}_{B,dis}$  is relevant for  $K < 3/2$  and is the leading perturbation in the model. In the RG analysis, the field-dependent localization length can be obtained,  $l_B \propto B^{-2/(3-2K)}$ .

- 
- [1] C. L. Kane and E. J. Mele, *Phys. Rev. Lett.* **95**, 146802 (2005).
  - [2] M. Z. Hasan and C. L. Kane, *Rev. Mod. Phys.* **82**, 3045 (2010).
  - [3] T. Senthil, *Annual Review of Condensed Matter Physics* **6**, 299 (2015) <https://doi.org/10.1146/annurev-conmatphys-031214-014740>
  - [4] C. L. Kane and E. J. Mele, *Phys. Rev. Lett.* **95**, 226801 (2005).
  - [5] B. A. Bernevig and S.-C. Zhang, *Phys. Rev. Lett.* **96**, 106802 (2006).
  - [6] L. Fu and C. L. Kane, *Phys. Rev. B* **79**, 161408 (2009).
  - [7] F. Zhang and C. L. Kane, *Phys. Rev. Lett.* **113**, 036401 (2014).
  - [8] C. P. Orth, R. P. Tiwari, T. Meng, and T. L. Schmidt, *Phys. Rev. B* **91**, 081406 (2015).
  - [9] J. Alicea and P. Fendley, *Annual Review of Condensed Matter Physics* **7**, 119 (2016).
  - [10] M. P. A. Fisher, P. B. Weichman, G. Grinstein, and D. S. Fisher, *Phys. Rev. B* **40**, 546 (1989).
  - [11] M. König, S. Wiedmann, C. Brüne, A. Roth, H. Buhmann, L. W. Molenkamp, X.-L. Qi, and S.-C. Zhang, *Science* **318**, 766 (2007).
  - [12] I. Knez, R.-R. Du, and G. Sullivan, *Phys. Rev. Lett.* **107**, 136603 (2011).

- [13] K. Suzuki, Y. Harada, K. Onomitsu, and K. Muraki, Phys. Rev. B **87**, 235311 (2013).
- [14] L. Du, I. Knez, G. Sullivan, and R.-R. Du, Phys. Rev. Lett. **114**, 096802 (2015).
- [15] T. Li, P. Wang, H. Fu, L. Du, K. A. Schreiber, X. Mu, X. Liu, G. Sullivan, G. A. Csáthy, X. Lin, and R.-R. Du, Phys. Rev. Lett. **115**, 136804 (2015).
- [16] F. Qu, A. J. A. Beukman, S. Nadj-Perge, M. Wimmer, B.-M. Nguyen, W. Yi, J. Thorp, M. Sokolich, A. A. Kiselev, M. J. Manfra, C. M. Marcus, and L. P. Kouwenhoven, Phys. Rev. Lett. **115**, 036803 (2015).
- [17] F. Nichele, H. J. Suominen, M. Kjaergaard, C. M. Marcus, E. Sajadi, J. A. Folk, F. Qu, A. J. Beukman, F. K. de Vries, J. van Veen, *et al.*, New Journal of Physics **18**, 083005 (2016).
- [18] B.-M. Nguyen, A. A. Kiselev, R. Noah, W. Yi, F. Qu, A. J. A. Beukman, F. K. de Vries, J. van Veen, S. Nadj-Perge, L. P. Kouwenhoven, M. Kjaergaard, H. J. Suominen, F. Nichele, C. M. Marcus, M. J. Manfra, and M. Sokolich, Phys. Rev. Lett. **117**, 077701 (2016).
- [19] F. Couëdo, H. Irie, K. Suzuki, K. Onomitsu, and K. Muraki, Phys. Rev. B **94**, 035301 (2016).
- [20] Z. Fei, T. Palomaki, S. Wu, W. Zhao, X. Cai, B. Sun, P. Nguyen, J. Finney, X. Xu, and D. H. Cobden, Nature Physics **13**, 677 (2017).
- [21] L. Du, T. Li, W. Lou, X. Wu, X. Liu, Z. Han, C. Zhang, G. Sullivan, A. Ikhlassi, K. Chang, and R.-R. Du, Phys. Rev. Lett. **119**, 056803 (2017).
- [22] E. Y. Ma, M. R. Calvo, J. Wang, B. Lian, M. Mühlbauer, C. Brüne, Y.-T. Cui, K. Lai, W. Kundhikanjana, Y. Yang, M. Baenninger, M. König, C. Ames, H. Buhmann, P. Leubner, L. W. Molenkamp, S.-C. Zhang, D. Goldhaber-Gordon, M. A. Kelly, and Z.-X. Shen, Nature communications **6** (2015).
- [23] C. Wu, B. A. Bernevig, and S.-C. Zhang, Phys. Rev. Lett. **96**, 106401 (2006).
- [24] C. Xu and J. E. Moore, Phys. Rev. B **73**, 045322 (2006).
- [25] H.-Y. Xie, H. Li, Y.-Z. Chou, and M. S. Foster, Phys. Rev. Lett. **116**, 086603 (2016).
- [26] S. F. Edwards and P. W. Anderson, Journal of Physics F: Metal Physics **5**, 965 (1975).
- [27] P. W. Anderson, Phys. Rev. **109**, 1492 (1958).
- [28] D. A. Huse, R. Nandkishore, V. Oganesyan, A. Pal, and S. L. Sondhi, Phys. Rev. B **88**, 014206 (2013).
- [29] R. M. Nandkishore and S. L. Sondhi, arXiv preprint arXiv:1705.06290 (2017).
- [30] S. A. Parameswaran and S. Gopalakrishnan, Phys. Rev. Lett. **119**, 146601 (2017).
- [31] T. Li, P. Wang, G. Sullivan, X. Lin, and R.-R. Du, arXiv preprint arXiv:1707.09024 (2017).
- [32] A. Ström, H. Johannesson, and G. I. Japaridze, Phys. Rev. Lett. **104**, 256804 (2010).
- [33] J. C. Budich, F. Dolcini, P. Recher, and B. Trauzettel, Phys. Rev. Lett. **108**, 086602 (2012).
- [34] T. L. Schmidt, S. Rachel, F. von Oppen, and L. I. Glazman, Phys. Rev. Lett. **108**, 156402 (2012).
- [35] R. Shankar, Acta Phys. Pol. B **26**, 1835 (1995).
- [36] T. Giamarchi, *Quantum physics in one dimension* (Oxford Science Publications, 2004).
- [37] R. Shankar, *Quantum Field Theory and Condensed Matter: An Introduction* (Cambridge University Press, 2017).
- [38] X.-L. Qi, T. L. Hughes, and S.-C. Zhang, Nature Physics **4**, 273 (2008).
- [39] R. Peierls, Mathematical Proceedings of the Cambridge Philosophical Society **55**, 311 (1958).
- [40] Y. Imry and S.-k. Ma, Phys. Rev. Lett. **35**, 1399 (1975).
- [41] V. L. Pokrovsky and A. L. Talapov, Phys. Rev. Lett. **42**, 65 (1979).
- [42] T. Giamarchi and H. J. Schulz, Phys. Rev. B **37**, 325 (1988).
- [43] N. Kainaris, I. V. Gornyi, S. T. Carr, and A. D. Mirlin, Phys. Rev. B **90**, 075118 (2014).
- [44] G. A. Fiete, K. Le Hur, and L. Balents, Phys. Rev. B **73**, 165104 (2006).
- [45] Y.-Z. Chou, A. Levchenko, and M. S. Foster, Phys. Rev. Lett. **115**, 186404 (2015).
- [46] M. Bocquet, Nuclear Physics B **546**, 621 (1999).
- [47] H. Fukuyama and P. A. Lee, Phys. Rev. B **17**, 535 (1978).
- [48] O. Narayan and D. S. Fisher, Phys. Rev. B **46**, 11520 (1992).
- [49] T. Giamarchi and P. Le Doussal, Phys. Rev. Lett. **76**, 3408 (1996).
- [50] L. Balents, M. C. Marchetti, and L. Radzihovsky, Phys. Rev. B **57**, 7705 (1998).
- [51] L. P. Gor'kov and G. Grüner, *Charge density waves in solids*, Vol. 25 (Elsevier, 2012).
- [52] Y. Imry, *Introduction to mesoscopic physics* (Oxford University Press on Demand, 2002).
- [53] V. Khemani, R. Nandkishore, and S. L. Sondhi, Nat. Phys. **11**, 560 (2015).
- [54] J. Maciejko, X.-L. Qi, and S.-C. Zhang, Phys. Rev. B **82**, 155310 (2010).
- [55] J. C. Y. Teo and C. L. Kane, Phys. Rev. B **79**, 235321 (2009).
- [56] C.-A. Li, S.-B. Zhang, and S.-Q. Shen, arXiv preprint arXiv:1709.01645 (2017).
- [57] R. Skolasinski, D. I. Pikulin, J. Alicea, and M. Wimmer, arXiv preprint arXiv:1709.04830 (2017).
- [58] D. I. Pikulin, T. Hyart, S. Mi, J. Tworzydło, M. Wimmer, and C. W. J. Beenakker, Phys. Rev. B **89**, 161403 (2014).
- [59] L.-H. Hu, D.-H. Xu, F.-C. Zhang, and Y. Zhou, Phys. Rev. B **94**, 085306 (2016).
- [60] J. I. Väyrynen, M. Goldstein, and L. I. Glazman, Phys. Rev. Lett. **110**, 216402 (2013).
- [61] J. I. Väyrynen, M. Goldstein, Y. Gefen, and L. I. Glazman, Phys. Rev. B **90**, 115309 (2014).
- [62] J. Maciejko, C. Liu, Y. Oreg, X.-L. Qi, C. Wu, and S.-C. Zhang, Phys. Rev. Lett. **102**, 256803 (2009).
- [63] Y. Tanaka, A. Furusaki, and K. A. Matveev, Phys. Rev. Lett. **106**, 236402 (2011).
- [64] J. I. Väyrynen, F. Geissler, and L. I. Glazman, Phys. Rev. B **93**, 241301 (2016).
- [65] B. L. Altshuler, I. L. Aleiner, and V. I. Yudson, Phys. Rev. Lett. **111**, 086401 (2013).